

## Electromagnetic Spin-Orbit Interactions via Scattering of Subwavelength Apertures

L. T. Vuong,<sup>1</sup> A. J. L. Adam,<sup>2</sup> J. M. Brok,<sup>3</sup> P. C. M. Planken,<sup>2</sup> and H. P. Urbach<sup>2,\*</sup>

<sup>1</sup>*School of Applied and Engineering Physics, Cornell University, Ithaca, New York, USA*

<sup>2</sup>*Optics Research Group, Delft University of Technology, The Netherlands*

<sup>3</sup>*Department of Mathematics and Computer Science, Eindhoven University of Technology, The Netherlands*

(Received 13 January 2009; published 24 February 2010)

Circularly polarized electric fields incident on subwavelength apertures produce near-field phase singularities with phase vorticity  $\pm 1$  depending on the polarization handedness. These near-field phase singularities combine with those associated with orbital angular momentum and result in polarization-dependent transmission. We produce arbitrary phase vorticity in the longitudinal component of scattered electric fields by varying the incident beam and aperture configuration.

DOI: [10.1103/PhysRevLett.104.083903](https://doi.org/10.1103/PhysRevLett.104.083903)

PACS numbers: 42.25.Fx, 42.25.Gy, 42.25.Ja, 42.50.Tx

Phase singularities in the electric field are locations at which the field amplitude is strictly zero. Given a fixed polarization or “spin”, the phase integral over the transverse field components enclosing a phase singularity provides a measure of the phase vorticity or orbital angular momentum (OAM) topological charge [1,2]. The three-dimensional electric field of an inhomogeneously polarized propagating electromagnetic wave produces three different types of polarization phase singularities [3], the evolution of which is studied in a rich array of literature [4]. Our understanding of phase singularities allows us to probe materials, characterize surfaces, study light propagation dynamics, and manipulate microparticles [5].

Within the last decade, there have been observations of near-field phase singularities (NFPS) in the evanescent waves produced by propagating [6] and scattered [7] light. The locations of NFPS produced by chiral “gammadion” [8] and spiral grating structures [9] depend on incident polarization handedness. These NFPS are connected to the extraordinary transmission of light through subwavelength slits [10], where whirlpool-like power flows and singularities in the Poynting vector are shown to exist [11,12]. Azimuthally and radially polarized vortices, beams with different polarization singularities, are transmitted through apertures with different efficiencies [13] but in spite of numerous measurements and observations of NFPS, the polarization-dependent transmission that occurs at subwavelength structures is not fully understood and light-metal interactions are neither fully optimized nor controlled.

Here, we show that the polarization-dependent transmission at sub-wavelength-structured materials are concisely explained by a coupling between electromagnetic spin and OAM. “Spin-orbit interactions” describe the modified light propagation due to their coupling where the longitudinal component of an electric field generally plays a crucial role. It has been shown that spin-orbit interactions occur via oblique reflections and refraction [14], in wave guiding structures [15], and in the focal plane

of highly focused beams [16]. In these situations, a change in either the direction of the phase vorticity or the polarization handedness results in a shift of the observed light intensity patterns.

Our work explains, for the first time, that polarization-dependent NFPS describe which modes and to what extent light is transmitted through thin-film apertures via the process of electromagnetic scattering. It was previously suggested that waveguiding due to the finite-thickness of material [13] is the primary mechanism responsible for polarization-dependent transmission through round subwavelength apertures. Our results suggest that the influence of incident polarization on the scattered-field phase is a non-negligible contribution. Numerical simulations verify our analytical predictions of polarization-dependent transmission and topological features and we reconstruct experimental THz field measurements with sub-wavelength-resolution that demonstrate polarization-dependent NFPS. Our insight of coherent light-metal interactions enables us to produce arbitrary phase vorticity in the longitudinal components of the scattered electric fields, which may enable new control of the surface currents in conducting thin films.

The topological charge or phase vorticity in the longitudinal or  $z$  component of a spin-polarized electric field is  $m_z = m_l + m_s$ , where  $m_l$  is the topological charge associated with OAM, and the topological charge associated with the photon spin number  $m_s = \pm 1$  depends on the orthogonal-spin polarization  $\sigma_{\pm}$ . This is illustrated by writing a continuous-wave circularly polarized field with transverse mode amplitude  $A(\rho, \phi, z)e^{im_l\phi}$  propagating in the  $\hat{\mathbf{k}}$  direction as

$$\tilde{\mathbf{E}} = [Ae^{im_l\phi}\hat{\sigma}_{\pm} + \Delta_{\pm}\hat{\mathbf{k}}]e^{i(\omega t - kz)}, \quad (1)$$

where the circular polarization unit vector is represented in Cartesian and cylindrical coordinates as  $\hat{\sigma}_{\pm} = (\hat{\mathbf{i}} \pm i\hat{\mathbf{j}})/\sqrt{2} = (\hat{\rho} \pm i\hat{\phi})e^{\pm i\phi}/\sqrt{2}$ . The longitudinal component of the electric field is calculated by Maxwell’s equation  $\hat{\mathbf{V}} \cdot \tilde{\mathbf{E}} = (\hat{\mathbf{V}}_{\perp} + \hat{\mathbf{d}}_z) \cdot \tilde{\mathbf{E}} = 0$ ,

$$\begin{aligned} \Delta_{\pm} e^{-ikz} &= - \int_{-\infty}^z e^{-ikz'} (\hat{\nabla}_{\perp} \cdot A' e^{im_l \phi} \hat{\sigma}_{\pm}) dz' \quad (2) \\ &= - \int_{-\infty}^z e^{-ikz'} \left[ (\hat{\partial}_{\rho} A') \pm \left( \frac{i \hat{\partial}_{\phi} - m_l}{\rho} A' \right) \right] dz' e^{i(m_l \pm 1) \phi}, \quad (3) \end{aligned}$$

where  $A' = A(\rho, \phi, z')$ . In Eq. (3), the topological charge of the longitudinal component of the electric field differs by one unit from that of the transverse components depending on the polarization handedness  $m_z = m_l \pm 1$  [3]. This polarization-dependent vortex phase in the longitudinal component is also referred to as a geometric or Rytov transformation phase [17–19], which is one source of spin-orbit interactions.

Spin-orbit interactions also arise because the spin and OAM density, which are proportional to the terms  $\text{Re}[\rho \hat{\partial}_{\rho} A]$  and  $\text{Re}[i \hat{\partial}_{\phi} A \exp(im_l \phi)]$  [1,20], manifest in Eq. (3) and add or cancel in the longitudinal-field component  $|\Delta_{\pm}|$ . Since the OAM contribution scales inversely with radius, this effect is significant when the distances between phase singularities and scattering edges are on the order of the incident-field wavelength. An analogous polarization-dependent coupling exists between a radially dependent phase and a nonradially symmetric intensity profile, i.e., imaginary valued bracketed terms of Eq. (3). We observe this effect in our investigation when a sample is not located in the focal plane of a normally incident field.

In this Letter, we explore optical spin-orbit interactions that occur due to the sharp edges of apertures. The longitudinal components of the transmitted electric fields, which are the focus of our investigation, arise via scattering or diffraction of subwavelength apertures and do not propagate to the far-field. We use an analytic mode solver [21] to numerically calculate the fields transmitted through apertures in ideal metal sheets with Cartesian symmetry. Figure 1 illustrates the longitudinal-field component at a distance  $\lambda/10$  after the metal sheet of thickness  $D = \lambda/2$ , produced by a normally incident left-handed or  $\sigma_+$  circularly polarized plane wave with zero OAM  $m_l = 0$  incident on a square aperture of length  $L = \lambda$ . The ampli-

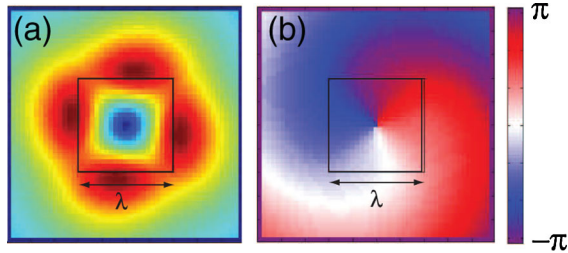


FIG. 1 (color online). Numerically calculated (a) amplitude and (b) phase of the scattered longitudinal-field component produced by a left-handed or  $\sigma_+$  circularly polarized plane wave incident on a square metal aperture of length  $L = \lambda$  and thickness  $D = \lambda/2$ .

tude [Fig. 1(a)] demonstrates electric-field enhancement at the aperture surfaces. The shadowside phase contains an NFPS of topological charge  $m_z = +1$  (clockwise, red-white-blue) [Fig. 1(b)]. The orthogonal  $\sigma_-$  or right-handed circularly polarized field produces the opposite topological charge  $m_z = -1$  (clockwise, blue-white-red) [not shown].

We experimentally measure the scattered longitudinal-field components from subwavelength apertures using a THz near-field electro-optic detection method and focused probe beam, which provides full vector characterization of the transmitted shadowside electric-field with  $10 \mu\text{m}$  resolution [22]. From the response to an incident linearly-polarized THz field and using the principle of superposition, we numerically reconstruct the response due to a circularly-polarized incident field. Figure 2 shows transmitted longitudinal-field amplitudes and phases produced by incident circularly-polarized field with wavelength  $\lambda = 500 \mu\text{m}$  on circular (radius  $a = 100 \mu\text{m}$ ) and square (length  $L = 200 \mu\text{m}$ ) apertures. Both square [Figs. 2(a) and 2(b)] and round [Figs. 2(c) and 2(d)] amplitudes show field enhancement due to interaction with aperture surfaces at the metal aperture edges, and the formation of an on-axis NFPS. Pairs of opposite-sign NFPS appear off-axis in Fig. 2(d), which we attribute to the non-normal angle of incidence between the incident field and the sample. Moreover, these off-axis NFPS associated with misalignment change in location depending on the incident  $\sigma_+$  or  $\sigma_-$  orthogonal-circular polarization.

The addition of an OAM topological charge  $m_l$  influences near-field scattering patterns and we consider input Laguerre-Gaussian profiles with index  $p = 0$

$$A^{(m_l)}(\rho_m, \phi, z = 0) = C \rho_m^{|m_l|} e^{-\rho_m^2/2} e^{im_l \phi}, \quad (4)$$

where  $C$  is a normalization constant such that  $\iint |A^{(m_l)}|^2 \rho_m d\rho_m d\phi = 1$ , or  $C = (m_l!/\pi)^{1/2}$ , and the radial coordinate  $\rho_m$  is normalized such that the mode field radius  $(\iint |A^{(m_l)}|^2 \rho_m^3 d\rho_m d\phi)^{1/2} = 1$ .

Figure 3 shows the amplitude and phase of the scattered longitudinal-field components for two orthogonal circularly polarized Laguerre-Gaussian beams, both with topological charge of  $m_l = +1$ . The mode field radius of the incident beam is one wavelength and outlined with dotted lines in Figs. 3(a) and 3(c) and the square aperture has length  $L = \lambda$ . We observe that the combination of left-

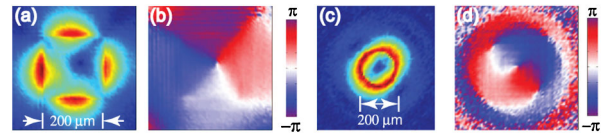


FIG. 2 (color online). The reconstructed amplitude and phase of scattered longitudinal-field components produced by (a)–(b) square and (c)–(d) round apertures in aluminum film when illuminated with an incident circularly polarized field with wavelength  $\lambda = 500 \mu\text{m}$ . The aperture width and radius are  $200 \mu\text{m}$ . The aluminum has a thickness of  $80 \mu\text{m}$ .

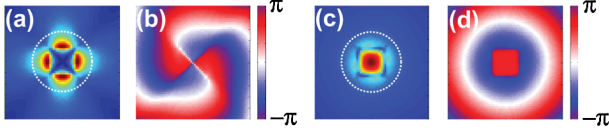


FIG. 3 (color online). Amplitudes and phases of the longitudinal-field component produced by Laguerre-Gaussian beams of topological charge  $m_0 = +1$  and (a)–(b) left-handed circular polarization and (c)–(d) right-handed circular polarization incident on square aperture  $L = \lambda$  and thickness  $D = \lambda/2$ . The dotted lines outline the incident mode field.

handed circular polarization and the incident vortex phase produces NFPS of  $m_z = +2$  [Fig. 3(b)]. In contrast, the combination of right-handed circular polarization with similar phase vorticity cancel and produce a flat-phase  $m_z = 0$  field [Fig. 3(d)]. A comparison of the amplitudes indicates that right-handed circular polarization [Fig. 3(c)] transmits an on-axis constructive maximum, whereas the amplitude of the left-handed circularly polarized scattered field is strictly zero on-axis due to the on-axis phase singularities [Fig. 3(a)]. Therefore, the addition of OAM breaks chiral symmetry and the near-field transmitted beam profiles associated with orthogonal-circular polarizations are no longer mirror images.

The coupling between spin polarization  $m_s$  and OAM  $m_l$  changes the energy that is scattered through apertures. From [23], the transmitted longitudinal-field component for an incident linearly polarized plane wave immediately behind a perfectly conducting aperture is

$$E_z(\rho, \phi) = \frac{4\rho}{\pi(a^2 - \rho^2)^{1/2}} [\cos\xi_0 \cos\theta_0 \cos\phi + \sin\xi_0 \sin\phi], \quad (5)$$

where  $\xi_0$  is the angle between the electric-field vector and the  $x$ - $z$  plane,  $a$  is the radius of the aperture,  $\rho$  and  $\phi$  are the cylindrical coordinates of the scattered field, and the incident angle  $\theta_0$  measures between the  $z$  axis and the direction of incidence,  $\mathbf{k}$ . Equation (5) provides an approximation of the scattered longitudinal-field components for the condition  $2\pi a/\lambda < 1$ . By decomposing the incident Laguerre-Gaussian beams [Eq. (4)] into linearly polarized plane waves with different wave vector  $\mathbf{k}$ , the corresponding  $\sigma_{\pm}$  transmitted field is obtained by superposition,

$$E_z^{(m_l, \sigma_{\pm})}(\rho_m, \phi) = \frac{C\rho_m e^{i(m_l \pm 1)\phi}}{\sqrt{a^2 - \rho_m^2} (|m_l| + 1)} \times \int_{k_\rho=0}^{k_\rho=k_c} (k_\rho)^{|m_l|} e^{-(k_\rho)^2/2} \times [(\kappa - 1)J_{|m_l \pm 2}(\rho_m k_\rho) - (1 + \kappa)J_{|m_l|}(\rho_m k_\rho)] k_\rho dk_\rho, \quad (6)$$

where the coefficient  $\kappa = \sqrt{1 - (k_\rho/k_m)^2}$  contains the normalized wavenumber  $k_m = 2\pi/\lambda\sqrt{|m_l| + 1}$ , and the cut-

off transverse wave number is  $k_c$ . For this investigation, we consider that plasmons are excited on the incident metal surface so that  $k_c = \infty$ ; a cutoff wave number of  $k_c = k_m$  implies that, for example, a dielectric coating prevents surface waves or plasmons from propagating on the incident metal surface. This  $\mathbf{k}$ -space relation Eq. (6), indicates that the scattered-field amplitudes couple into Bessel functions of order  $m_l$  and  $m_l \pm 2$ , while the NFPS remains described by the relation  $m_z = m_l + m_s = m_l \pm 1$ . The electromagnetic spin-orbit interaction exists in the Bessel term  $J_{m_l \pm 2}$ , which indicates that the energy scattered through the aperture depends on both spin  $m_s$  and OAM  $m_l$ .

In Fig. 4 we show the difference in transmission associated with each orthogonal polarization  $\Delta T = (T_+ - T_-)/(T_+ + T_-)$  for varying OAM topological charge  $m_l$  as a function of aperture diameter or length  $L = 2a$ , where the transmission is  $T_{\pm} = \iint |E_z^{(m_l, \sigma_{\pm})}(\rho_m, \phi)|^2 \rho_m d\rho_m d\phi$ . The aperture width is normalized by the input beam mode field diameter and since there is no cutoff transverse wave number  $k_c = \infty$ , our analytical calculation is independent of wavelength. Theoretical predictions are shown in Fig. 4(a). In Fig. 4(b), we plot the difference in transmission from numerical simulations for metal sheet thickness  $D = \lambda$  and polynomial curve-fit lines. The difference in transmission  $\Delta T$  represents the spin-orbit interaction via electromagnetic scattering and is therefore zero when there is no OAM present or  $m_l = 0$ .

The difference in transmission  $\Delta T$  for a single incident vortex  $m_l = 1$  is less than 10%, while that for higher-order vortices exceeds 50% depending on aperture size. Both numerical calculations and theoretical analysis predict similar aperture sizes for maximum spin-orbit interaction or maximum  $|\Delta T|$ . We observe a maximum spin-orbit interaction for  $m_l = 2$  when aperture sizes approach zero, and the maximum spin-orbit interactions occur for increasing  $m_l$  at increasing aperture widths. Our theoretical prediction strongly underestimates the difference in transmission, particularly at small aperture sizes, and this is not reconciled by changing the metal sheet thickness in nu-

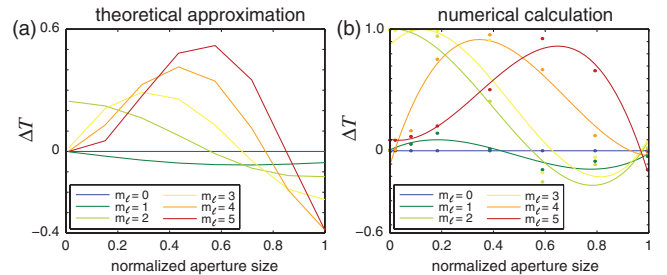


FIG. 4 (color online). Difference in transmission between orthogonal circularly polarized vortices  $\Delta T = (T_+ - T_-)/(T_+ + T_-)$  as a function of normalized hole aperture size for different incident topological charge  $m_l$ . (a) Theoretical prediction given a round aperture in an infinitely thin metal sheet. (b) Numerical calculation for a square aperture given finite sheet thickness  $D = \lambda$ . Note: graphs use different scales.

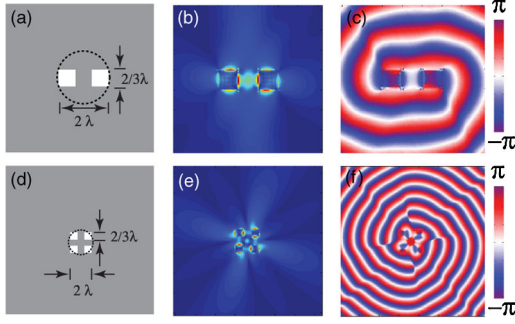


FIG. 5 (color online). (a, d) Two- and four-aperture configurations with dimensions and separation  $L = 2/3\lambda$ . (b), (e) Amplitude and (c), (f) phase of the corresponding scattered-field longitudinal components via numerical calculations. The metal sheet has thickness  $D = \lambda/4$ . The dotted lines outline the incident mode field.

merical simulations. Discrepancies arise from the comparison between cylindrical (theoretical) and Cartesian (numerical) symmetry, however this point does not entirely resolve the differences described. Polarization-dependent singularities exist in both near and far fields, however the spin-orbit interaction  $\Delta T$  that we investigate appears to exist only in the near field.

Thus far in this Letter we have described the NFPS produced by a single aperture. If a  $\sigma_{\pm}$ -polarized plane wave instead illuminated  $n$  apertures, then each aperture would produce a NFPS of  $m_z = \pm 1$ , however an additional  $(n - 1)$  NFPS with *opposite* sign  $\mp 1$  would also arise. The net topological charge  $m_z$ , determined by a phase integral along a path enclosing the  $m$  apertures, would remain conserved and follow the relation  $m_z = m_s = \pm 1$ .

Yet arbitrary phase vorticity  $m_z$  in the longitudinal-field components can be achieved by manipulating the Berry-Rytov phase source term in Eq. (3). We demonstrate this here by using a “necklace” arrangement of  $n$  apertures, where  $n$  corresponds to the desired phase vorticity  $m_z$ , and prepare the input field polarization as

$$\hat{\mathbf{e}}_{\pm}^V(\phi) = e^{i\mp\phi} \hat{\boldsymbol{\sigma}}_{\pm} \quad (7)$$

$$= \frac{1}{\sqrt{2}} (\hat{\boldsymbol{\rho}} \pm i\hat{\boldsymbol{\phi}}). \quad (8)$$

This polarization vector is a superposition of radially and azimuthally polarized fields. It is also the spin-polarization vector  $\hat{\boldsymbol{\sigma}}_{\pm}$  with a single on-axis phase singularity. We use Laguerre-Gaussian profiles  $|A^{(m_l=1)}|$ , however, we observe that the amplitude of the incident field does not substantially affect the phase of the scattered fields. With a  $\hat{\mathbf{e}}_{\pm}^V$ -polarized field centered and incident on an azimuthal arrangement of  $n$  apertures, transmission through each individual aperture produces a single topological charge whose sign is determined by the local  $\pm$  handedness in Eq. (8). The total topological charge  $m_z = nm_s$  is defined by a phase integral on a path enclosing the apertures. In Figs. 5(a) and 5(d) we show  $n = 2$  and  $n = 4$  equally spaced square holes separated by and with dimen-

sions  $L = 2/3\lambda$ . Figs. 5(b) and 5(e) show the amplitudes and Figs. 5(c) and 5(f) illustrate the phases with  $m_z = +2m_s$  and  $m_z = +4m_s$  using an incident polarization  $\hat{\mathbf{e}}_{+}^V$  when the metal sheet has thickness  $D = \lambda/4$ . We remark that the same  $\hat{\mathbf{e}}_{+}^V$  polarized field incident on a single on-axis aperture would produce near-field amplitude and phase profiles that mirror Figs. 3(c) and 3(d).

In conclusion, electromagnetic spin and OAM NFPS combine and change the near-field energy that is scattered through round and square subwavelength apertures. Depending on the aperture size and incident phase vorticity, the difference in transmission due to polarization can exceed 50%. Our research indicates that planar asymmetric or chiral metal nanostructures that change the polarization of scattered fields also impart a phase vorticity and this explains previously observed polarization-dependent spatial beam profiles [8–10]. Our results illuminate new considerations for manipulating plasmons or surface waves, and designing or aligning metamaterials.

The author graciously acknowledges funding from the Fulbright and Netherlandic-American Foundations via Philips Electronics North America. Aperture samples were provided by M. A. Seo and D. S. Kim.

\*Luat.Vuong@icfo.es

- [1] L. Allen *et al.*, *Prog. Opt.* **39**, 291 (1999).
- [2] M. S. Soskin and M. V. Vasnetsov, *Prog. Opt.* **42**, 219 (2001).
- [3] M. V. Berry and M. R. Dennis, *Proc. R. Soc. A* **457**, 141 (2001); M. R. Dennis, *Opt. Commun.* **213**, 201 (2002).
- [4] M. V. Berry and M. R. Dennis, *J. Phys. A* **40**, 65 (2007); R. W. Schoonover and T. D. Visser, *Opt. Express* **14**, 5733 (2006).
- [5] H. He *et al.*, *Phys. Rev. Lett.* **75**, 826 (1995).
- [6] M. L. M. Balistreri *et al.*, *Phys. Rev. Lett.* **85**, 294 (2000).
- [7] A. Nesci *et al.*, *Opt. Commun.* **205**, 229 (2002).
- [8] A. Papakostas *et al.*, *Phys. Rev. Lett.* **90**, 107404 (2003); M. Kuwata-Gonokami *et al.*, *Phys. Rev. Lett.* **95**, 227401 (2005).
- [9] T. Ohno and S. Miyanishi, *Opt. Express* **14**, 6285 (2006).
- [10] A. V. Krasavin *et al.*, *J. Opt. A* **8**, S98 (2006).
- [11] M. V. Bashevoy *et al.*, *Opt. Express* **13**, 8372 (2005).
- [12] H. F. Schouten *et al.*, *Phys. Rev. Lett.* **93**, 173901 (2004).
- [13] J. Kindler *et al.*, *Appl. Phys. B* **89**, 517 (2007).
- [14] R. Y. Chiao *et al.*, *Phys. Rev. Lett.* **60**, 1214 (1988).
- [15] V. S. Liberman and B. Y. Zeldovich, *Phys. Rev. A* **46**, 5199 (1992); A. Yu Savchenko and B. Ya Zeldovich, *J. Opt. Soc. Am. B* **13**, 273 (1996).
- [16] B. Y. Zeldovich *et al.*, *JETP Lett.* **59**, 766 (1994); K. Lindfors *et al.*, *Nat. Photon.* **1**, 228 (2007).
- [17] S. M. Rytov, *Dokl. Akad. Nauk SSSR* **18**, 263 (1938).
- [18] M. V. Berry, *Proc. R. Soc. A* **392**, 45 (1984).
- [19] K. Y. Bliokh, *Phys. Rev. Lett.* **97**, 043901 (2006).
- [20] A. T. O’Neil *et al.*, *Phys. Rev. Lett.* **88**, 053601 (2002).
- [21] J. M. Brok and H. P. Urbach, *Opt. Express* **14**, 2552 (2006).
- [22] A. J. L. Adam *et al.*, *Opt. Express* **16**, 7407 (2008).
- [23] C. J. Bouwkamp, *Rep. Prog. Phys.* **17**, 35 (1954).